THE JOURNAL OF PHYSICAL CHEMISTRY A

pubs.acs.org/JPCA Article

Comparison of the Photochemistry of Acyclic and Cyclic 4-(4-Methoxy-phenyl)-4-oxo-but-2-enoate Ester Derivatives

Sujan K. Sarkar,[†] Ranaweera A. A. Upul Ranaweera,[†] Rajkumar Merugu,[†] Nayera M. Abdelaziz, Jendai Robinson, Heidi A. Day, Jeanette A. Krause, and Anna D. Gudmundsdottir*

Cite This: *J. Phys. Chem. A* 2020, 124, 7346−7354 Read Online

ACCESS | Metrics & More | Article Recommendations | Supporting Information

ABSTRACT: To clarify the cis−trans isomerization mechanism of simple alkenes on the triplet excited state surface, the photochemistry of acyclic and cyclic vinyl ketones with a *p*-methoxyacetophenone moiety as a built-in triplet sensitizer (**1** and **2**, respectively) was compared. When irradiated, ketone **1** produces its cis-isomer, whereas ketone **2** does not yield any photoproducts. Laser flash photolysis of ketone **1** yields a transient spectrum with $\lambda_{max} \sim 400$ nm ($\tau \sim 125$ ns). This transient is assigned to the first triplet excited state (T_1) of **1**, which presumably decays to form a triplet biradical (**1BR**) that is shorter lived than the triplet ketone. In comparison, laser flash photolysis of **2** reveals two transients ($\tau \sim 20$ and 440 ns), which are assigned to T_1 of **2** and triplet biradical **2BR**, respectively. Density functional theory calculations support the characterization of the triplet excited states and the biradical intermediates formed upon irradiation of ketones **1** and **2** and allow a comparison of the physical properties of the biradical intermediates. As the biradical centers in **2BR** are stabilized by conjugation, **2BR** is more rigid than **1BR**. Therefore, the longer lifetime of **2BR** can be attributed to less-efficient intersystem crossing to the ground state.

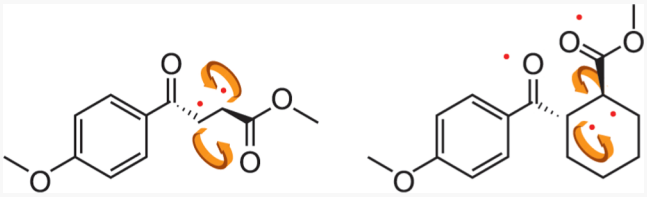

1. INTRODUCTION

The light-induced cis−trans isomerization of simple alkene derivatives is of general interest because of its utility in various applications.[1] For example, the light-activated cis−trans isomerization of overcrowded alkenes has been successfully used to make numerous molecular motors.[2] Similarly, the cis−trans isomerization of alkene derivatives has been used to trigger photoswitches.[2] Furthermore, this process has also been applied to initiate the release of photoremovable protecting groups.[3−5] To be able to design and develop a broad array of applications that rely on the cis−trans isomerization of simple alkenes, it is important to understand their isomerization mechanism. It has been shown that the cis−trans isomerization of simple alkenes can occur on both their singlet or triplet excited state surfaces.[6] On the triplet surface, the cis−trans isomerization goes through twisted triplet 1,2-biradicals.[7] The twisted geometry of the triplet 1,2-biradicals is favored because it reduces the electronic repulsion between the two unpaired electrons on the adjacent carbon atoms. However, twisted biradicals have been studied sporadically because most simple alkenes do not intersystem-cross to the triplet excited state efficiently. In particular, the large energy gap between the singlet and triplet excited states of simple alkenes restricts efficient intersystem crossing. To bypass this limitation, Caldwell et al. used the intermolecular sensitization of stilbene derivatives to form 1,2-biradicals (Scheme 1).[8] These biradicals had lifetimes of ∼ 100 ns unless they were incorporated into a cyclic structure, in which case, they

Scheme 1. Intermolecular Sensitization of Alkene Derivatives to Form Twisted Triplet 1,2-Biradicals

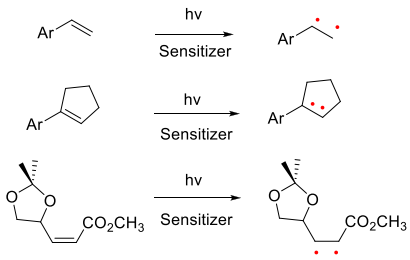

become longer lived with lifetimes of a few microseconds. Furthermore, García-Expósito et al. demonstrated that the intermolecular sensitization of simple alkene ester derivatives can also be used to form triplet 1,2-biradicals (Scheme 1).[9]

These authors demonstrated that the twisted biradicals decay by intersystem crossing to the ground state, forming the corresponding cis- or trans-isomers. The energy gap between the triplet biradical and the singlet ground state is minimized for the twisted conformer of the 1,2-biradical. However,

Received: May 13, 2020
Revised: July 20, 2020
Published: August 5, 2020

https://dx.doi.org/10.1021/acs.jpca.0c04319
J. Phys. Chem. A 2020, 124, 7346−7354

intersystem crossing is enhanced by spin−orbit coupling, which is insignificant in the twisted conformer. Thus, they theorized that intersystem crossing occurs where the two radical centers are orientated ∼45° apart, where spin−orbit coupling is more significant. More recently, Ranaweera et al. and Sriyarathne et al. demonstrated that the cis−trans isomerization of simple alkenes with built-in acetophenone triplet sensitizers also takes place through triplet 1,2-biradicals.[10,11]

In this paper, we report the photochemistry of vinyl ketones **1** and **2**, in which the vinylic bond is conjugated to an ester moiety and a *p*-methoxyacetophenone chromophore that serves as a built-in triplet sensitizer. In addition, the vinylic bond of ketone **2** is part of a ring structure, therefore making it possible to determine the effect of conjugation on cis−trans isomerization of simple acyclic and cyclic alkenes. Density functional theory (DFT) calculations were performed to support the characterization of the excited states and intermediates as well as the proposed reaction mechanism.

2. EXPERIMENTAL SECTION

2.1. Calculations. DFT calculations were performed using Gaussian16 at the B3LYP level of theory and with the 6-31+G(d) basis set to optimize the structures of the ground states (S_0 of **1**, S_0 of **2**), excited states (T_1 of **1**, T_1 of **2**), triplet intermediates (**1BR** and **2BR**), and photoproduct (*cis*-**1**).[12,13] Single point time-dependent density functional theory (TD-DFT) calculations (B3LYP/6-31+G(d)) were used to estimate the vertical energies of the first singlet state (S_1) and T_1 of **1** and **2**, and to calculate the absorption spectra of T_1 of **1**, T_1 of **2**, triplet **1BR**, and triplet **2BR**, using the conductor-like polarizable continuum model for solvation and acetonitrile as the solvent.[14−19] All transition states were confirmed to have one imaginary vibrational frequency by the analytical determination of the second derivative of the energy with respect to the internal coordinates. Intrinsic reaction coordinate calculations were used to verify that the transition state correlates the reagent and product.[20,21]

2.2. Laser Flash Photolysis. Laser flash photolysis was performed using an excimer laser (308 nm, 17 ns); this system has previously been described in detail.[22] A stock solution of **1** was prepared in spectroscopic-grade acetonitrile. The concentration of the stock solution was such that the ground state absorbance was between 0.3 and 0.8 at 308 nm. For the laser flash photolysis measurements, quartz cuvettes with a 10 mm × 10 mm cross section were used. Approximately, 2 mL of the stock solution was placed in the cuvette, which was then purged with argon or oxygen for the required time.

Transient absorption measurements were performed using a commercially available laser flash photolysis instrument (LP980, Edinburgh Instruments, Inc.) with laser excitation (266 nm, 6−7 mJ, 8 mm diameter, 3−5 ns fwhm, 10 Hz) provided by a pulsed neodymium-doped yttrium aluminum garnet (Nd:YAG) laser (Surelite II, Continuum, Inc.). White light was used as a probe to monitor the kinetics and transient absorption spectra. The LP980-K PMT detector (repetition rate of 10 Hz for single shot pulses, current up to 100 A, and pulse duration of 0.2−6 ms) was used for the kinetics measurements. The kinetic traces were collected by averaging the data from 40 to 80 laser shots using a spectral gate width between 0.5 and 2 nm and a PMT potential of less than 600 mV. The LP980-KS PMT detector with an externally triggered, optimized gated ICCD camera (7 ns (fwhm), 960 × 256 pixels, −20 °C, 3 ns minimum optical gate width) was used for spectral measurements. The transient absorption spectra were collected by averaging the data from 60 laser shots for each time window using a spectral band width between 1 and 2 nm, gate delay with 0 ns, gate width at 50 and 100 ns, a gain between 1600 and 2200, and CCD spectrum map counts of less than 30,000. The data were converted to a text file in the L900 software and then plotted and analyzed in the IgorPro software.

For the experiments using the Nd:YAG laser for excitation, a home-built flow cell was employed where the irradiation occurred in a cell with a 10 × 4 × 11 mm ($L \times W \times H$) inner diameter and outer chamber parameters of 12.5 × 12.5 × 45 mm. A pump was used to pump the solution through the cell and a reservoir, which was continuously purged with argon or oxygen.

2.3. Synthesis of Ketones 1 and 2. *2.3.1. Synthesis of Ketone 1. 2.3.1.1. (E)-4-(4-Methoxy-phenyl)-4-oxo-but-2-enoic Acid.* Anisole (5.461 g, 50.00 mmol) was dissolved in dichloromethane (30 mL), and then, maleic anhydride (7.505 g, 75 mmol, 1.5 equiv) and $AlCl_3$ (9.900 g, 75 mmol, 1.5 equiv) were added. The reaction was stirred for 20 h at ambient temperature, extracted with dichloromethane (50 mL), and then washed with water three times (50 mL) and with saturated brine solution once (100 mL). The organic layer was dried over anhydrous $MgSO_4$ and the solvent removed under vacuum to yield 4-(4-methoxy-phenyl)-4-oxo-but-2-enoic acid as a yellow solid (5.09 g, 25 mmol, 50% yield). The ^{1}H NMR spectrum of the crude was consistent with published data.[23−25]

mp 135.1−135.9 °C (lit.[24] 135−136 °C); ^{1}H NMR (400 MHz, $CDCl_3$): δ 8.05−7.97 (m, 2H), 7.29−7.26 (m, 1H), 7.04−6.90 (m, 2H), 6.874 (d, J = 15.6 Hz, 1H), 3.904 (s, 3H) ppm.

2.3.1.2. 4-(4-Methoxy-phenyl)-4-oxo-but-2-enoic Acid Methyl Ester (1). 4-(4-Methoxy-phenyl)-4-oxo-but-2-enoic acid (5.09 g, 25 mmol) was dissolved in methanol (30 mL), and then, a catalytic amount of *p*-toluenesulfonic acid was added. After stirring the reaction for 20 h while refluxing, diethyl ether (50 mL) and water (50 mL) were added. The organic layer was washed twice with water (50 mL) and once with saturated brine (100 mL). The organic layer was dried over anhydrous $MgSO_4$ and the solvent removed under pressure to yield **1** as a yellow solid (1.56 g, 7 mmol, 28% yield). The NMR and IR spectra of **1** are consistent with those reported previously.[26]

^{1}H NMR (400 MHz, $CDCl_3$): δ 8.01 (d, J = 8.8 Hz, 2H, −CH), 7.94 (d, J = 15.6 Hz, 1H), 6.99 (d, J = 8.8 Hz, 2H, −CH), 6.88 (d, J = 15.6 Hz, 1H), 3.90 (s, 3H, $-OCH_3$), 3.85 (s, 3H, $-OCH_3$) ppm; ^{13}C NMR (100 MHz, $CDCl_3$): δ 187.5, 166.2, 164.3, 136.8, 131.3, 130.8 129.7, 114.1, 55.6, 52.3 ppm; IR ($CDCl_3$): 3064, 3029, 2954, 2844, 1716, 1668, 1626, 1593, 1512, 1458, 1445, 1420, 1337, 1305, 1265, 1198, 1164, 1116, 1027, 984, 942, 832, 766, 714, 689, 632, 596 cm^{-1}; GC/MS (EI): m/z 220 (M^+), 205, 189, 177, 161, 146, 135 (100%), 129, 118, 107, 101, 92, 85, 77, 64, 54.

2.3.2. Synthesis of Ketone 2. 2.3.2.1. Methyl-2-((4-methoxyphenyl)carbonyl)cyclohex-1-ene-1-carboxylate (2).[26,27] 4,5,6,7-Tetrahydro-2-benzofuran-1,3-dione (6.20 g, 40.75 mmol) was placed in a 250 mL round-bottomed flask and dissolved in dichloromethane (100 mL). Anisole (4.03 mL, 37.05 mmol) was added to this solution, followed by the slow addition of dry aluminum chloride (12.35 g, 92.63

https://dx.doi.org/10.1021/acs.jpca.0c04319
J. Phys. Chem. A 2020, 124, 7346−7354

mmol). The mixture was stirred at 0 °C for approximately 2 h and then kept at room temperature overnight. The reaction mixture was quenched with ice-cold water, and diluted HCl (1 N) was added dropwise until the pH was ∼5. The organic layer was extracted with dichloromethane and washed with water. The organic layer was dried over $MgSO_4$, and the solvent was removed under reduced pressure to produce crude acid, which was used for the next step without any further purification. Crude acid (6.72 g, 25.85 mmol) was dissolved in 50 mL of methanol, and then, a catalytic amount of concentrated sulfuric acid (∼15 drops) was added. After stirring the reaction mixture at room temperature for 1 day, the solvent was removed under vacuum. The resulting reddish oil was extracted with diethyl ether (50 mL) and washed with water (50 mL) three times. The organic layer was dried over $MgSO_4$ and the solvent removed under reduced pressure to yield a crude red liquid. The crude product was purified on a silica column (eluted with 10:90 (v/v) ethyl acetate/hexane) to yield **2** as a pure white solid (1.82 g, 6.64 mmol, 26% yield). The final product was characterized by X-ray crystallography (see Supporting Information for details CCDC-2003612), ^{1}H and ^{13}C NMR spectroscopy, IR spectroscopy, and high-resolution mass spectrometry (HR-MS).

mp 88.0−90.1 °C; ^{1}H NMR (400 MHz, $CDCl_3$): δ 7.85−7.83 (m, 2H), 6.95−6.93 (d, J = 8 Hz, 2H), 3.87 (s, 3H), 3.48 (s, 3H), 2.45−2.44 (br d, 2H), 2.36−2.35 (br d, 2H), 1.76−1.75 (br d, 4H) ppm; ^{13}C NMR (400 MHz, $CDCl_3$): δ 198, 167, 164, 150, 131, 128, 127, 114, 55, 52, 29, 25, 22, 21 ppm; IR ($CDCl_3$): 2939, 2861, 2842, 1769, 1716, 1663, 1599, 1577 cm^{-1}; HR-ESI-MS: 275.1288 (experimental), 275.1283 (theoretical); m/z 275, 243 (100%), 167.

2.4. Photolysis. *2.4.1. Photolysis of Trans-1.* A solution of *trans*-**1** (∼20 mg, 0.1 mmol) in $CDCl_3$ (2 mL) in a NMR tube was purged with argon for 5 min and photolyzed using a medium-pressure mercury lamp through a Pyrex filter for 16 h at 298 K. After 16 h, ^{1}H NMR analysis of the reaction mixture showed complete conversion to cis-**1** (100%). The product was characterized by gas chromatography (GC)−MS and ^{1}H NMR spectroscopy without further purification. The NMR spectrum of *cis*-**1** was consistent with that reported in the literature.[28]

cis-**1**: ^{1}H NMR (400 MHz, $CDCl_3$): δ 7.91 (d, J = 8.8 Hz, 2H), 6.96−6.93 (m, 3H), 6.26 (d, J = 12 Hz, 1H), 3.88 (s, 3H, $-OCH_3$), 3.62 (s, 3H) ppm; ^{13}C NMR (100 MHz, $CDCl_3$): δ 192.6, 165.4, 164.0, 141.5, 131.1, 128.9, 125.3, 114.0, 55.5, 51.9 ppm; IR ($CDCl_3$): 2952, 2841, 1726, 1664, 1650, 1598, 1576, 1511, 1458, 1437, 1420, 1387, 1306, 1254, 1220, 1163, 1113, 1021, 993, 913, 849, 822, 796, 743, 650, 602 cm^{-1}; GC/MS (EI): m/z 220 (M^+), 189, 174, 161, 146, 135 (100%), 120, 113, 107, 92, 85, 77, 64, 54.

2.4.2. Photolysis of 2. A solution of ketone **2** (0.020 g, 0.073 mmol) in acetonitrile-d_3 (5 mL) in a test tube was purged with argon for 8 min. The resulting solution was photolyzed with a medium-pressure mercury lamp through a Pyrex filter for 2 days. The ^{1}H NMR spectrum of the irradiated solution did not reveal the formation of any new products.

2.5. Phosphorescence. Ethanol solutions of **1** (0.01 M) and **2** (0.01 M) were prepared and cooled to 77 K. The phosphorescence spectra of the ethanol glasses of **1** and **2** were obtained using a phosphorimeter, which has previously been described in detail.[11] The excitation wavelength was 266 nm, and the emission spectra were recorded between 280 and 800 nm.

3. RESULTS

3.1. Product Studies. The photoreactivity of ketones **1** and **2** was monitored by ^{1}H NMR spectroscopy. Irradiations of trans-**1** through a Pyrex filter for 16 h in argon-saturated chloroform-*d* resulted in complete conversion to *cis*-**1** (Scheme 2). In contrast, photolysis of ketone **2** did not result in any photoproducts.

Scheme 2. Photolysis of 1 and 2 in Argon-Saturated Solutions

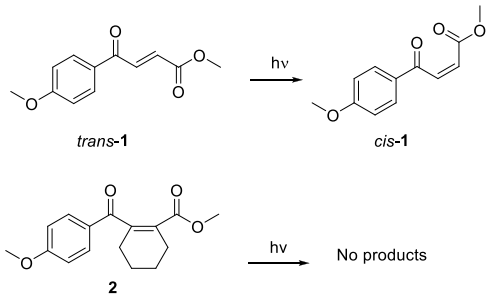

Because **1** and **2** have a *p*-methoxyacetophenone moiety as a built-in triplet sensitizer, we propose that upon excitation, they form their T_1, which decays to form the corresponding twisted triplet 1,2-biradical (**1BR** and **2BR**, respectively). Biradical **1BR** intersystem-crosses to form *cis*-**1** and presumably also reforms the starting material; however, prolonged irradiation yields *cis*-**1**, selectively. In contrast, the ring structure of biradical **2BR** restricts it to reformation of the starting material (Scheme 3).

3.2. Laser Flash Photolysis. We used laser flash photolysis to support the proposed mechanism for the photoreactivity of ketones **1** and **2** (Scheme 3). Laser flash photolysis (266 nm) of *trans*-**1** in argon-saturated acetonitrile showed a broad transient absorption with λ_{max} at ∼400 nm (Figure 1a). Kinetic traces at 400 nm showed that the transient formed within the laser pulse, and its decay was best-fitted as a monoexponential function with a rate constant of 7.97 × 10^6 s^{-1} (τ = 125 ns, Figure 1c). The transient absorption was fully quenched in oxygen-saturated acetonitrile.

We assign the observed transient absorption to T_1 of **1** based on the similarity between the transient absorption spectra and the calculated electronic transitions. TD-DFT calculations showed that the major electronic transitions for T_1 of **1** above 300 nm are located at 474 (oscillator strength (f) = 0.1742), 427 (f = 0.0657), and 380 (0.3917) nm (Figure 1b), which correspond well to the observed spectra (Figure 1a). In comparison, the major electronic transitions calculated for **1BR** (350 (f = 0.0427) and 338 (f = 0.017) nm) do not fit as well with the observed transient spectra.

To further support the assignment of the transient absorption to T_1 of **1**, quenching studies were performed using isoprene. The lifetime of T_1 of **1** decreased as the isoprene concentration increased. A plot of the rate of decay of T_1 of **1** versus the isoprene concentration gave a straight line with a slope of 5.8 × 10^9 M^{-1} s^{-1} (Figure 2), thus revealing that T_1 of **1** is quenched with a rate constant approaching the diffusion-controlled limit, as expected for a triplet ketone.[29]

Therefore, we propose that T_1 of **1** is short-lived because it decays efficiently to form **1BR**, which intersystem-crosses to form *cis*-**1**. In contrast, the triplet excited state of *p*-methoxyacetophenone has been reported to have a lifetime

https://dx.doi.org/10.1021/acs.jpca.0c04319
J. Phys. Chem. A 2020, 124, 7346−7354

Scheme 3. Proposed Mechanism for the Photoreactivity of Ketones 1 and 2

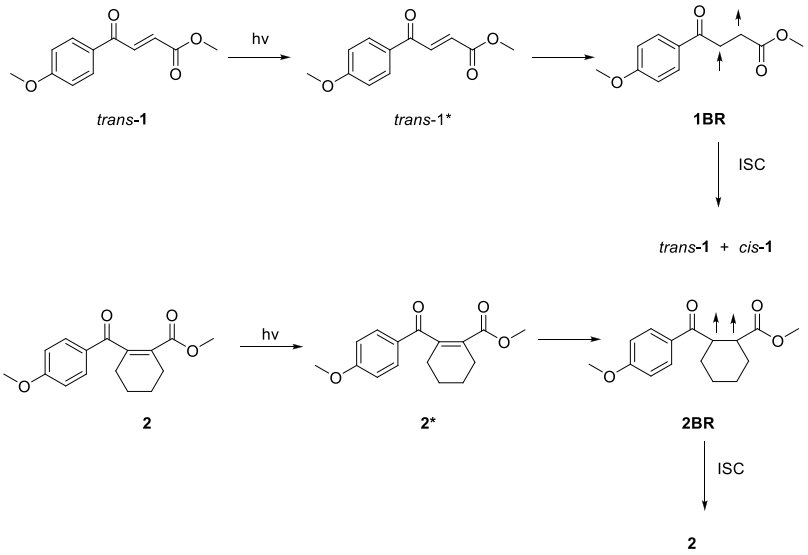

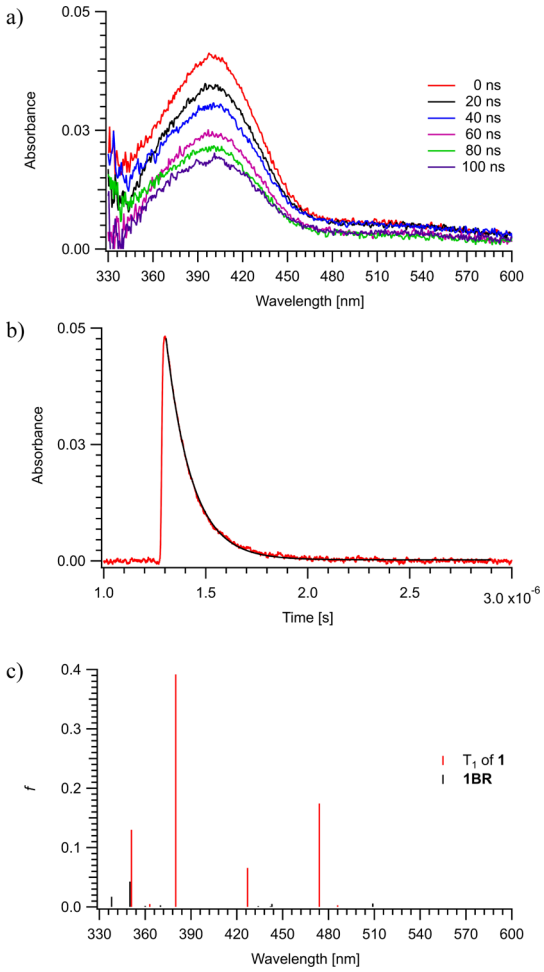

Figure 1. (a) Transient absorption spectra obtained by laser flash photolysis of **1** in argon-saturated acetonitrile using a 266 nm Nd:YAG laser. (b) Kinetic trace at 400 nm obtained by laser flash photolysis of **1**in argon-saturated acetonitrile. (c) TD-DFT-calculated electronic transitions for $T_1$of **1**and **1BR**.

of a few microseconds in solution.[30] Because we do not observe **1BR**, we theorize that **1BR** is shorter-lived than T_1 of

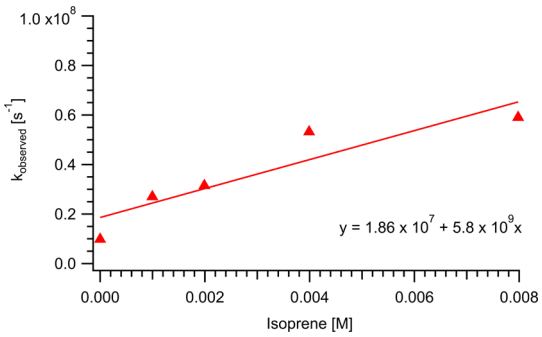

Figure 2. Quenching plot for the rate of decay of T_1 of **1** vs isoprene concentration.

1. In other words, the rate-limiting step is the decay of T_1 of **1** to **1BR**. However, we cannot rule out the possibility that the absorption of **1BR** is too weak to be detected directly.

In comparison, laser flash photolysis of ketone **2** in argon-saturated acetonitrile resulted in a transient spectrum with λ_{max} ~ 320 nm, which trails out to 380 nm (Figure 3a). The transient absorption was fully quenched in oxygen-saturated acetonitrile. Kinetic traces at 360 nm mainly showed a short-lived decay that could be fitted as a monoexponential function to yield a rate constant of 5.01×10^7 s^{-1} (τ = 20 ns) (Figure 3c). In contrast, the decay at 320 nm could be fitted as a biexponential function, and when one of the components was fixed to the rate constant obtained at 360 nm, a slower rate constant of 2.28×10^6 s^{-1} (τ = 440 ns) was obtained (Figure 3b). We assign the shorter-lived component to T_1 of **2** and the longer-lived one to **2BR**. TD-DFT calculations further supported these assignments, as the major electronic transitions for **2BR** are located at 304 (f = 0.0331), 358 (f = 0.1087), and 440 (f = 0.0256) nm, whereas those for T_1 of **2** are located at 294 (f = 0.2821), 312 nm (f = 0.1308), and 354 (f = 0.2098) nm (Figure 3d). These calculated transitions correspond adequately to the observed spectra.

The assignment of the transient absorption of T_1 of **2** was further supported by isoprene quenching studies, as described to for T_1 of **1**. A plot of the rate of decay of T_1 of **2** versus the isoprene concentration gave a straight line with a slope of 2.65

https://dx.doi.org/10.1021/acs.jpca.0c04319
J. Phys. Chem. A 2020, 124, 7346−7354

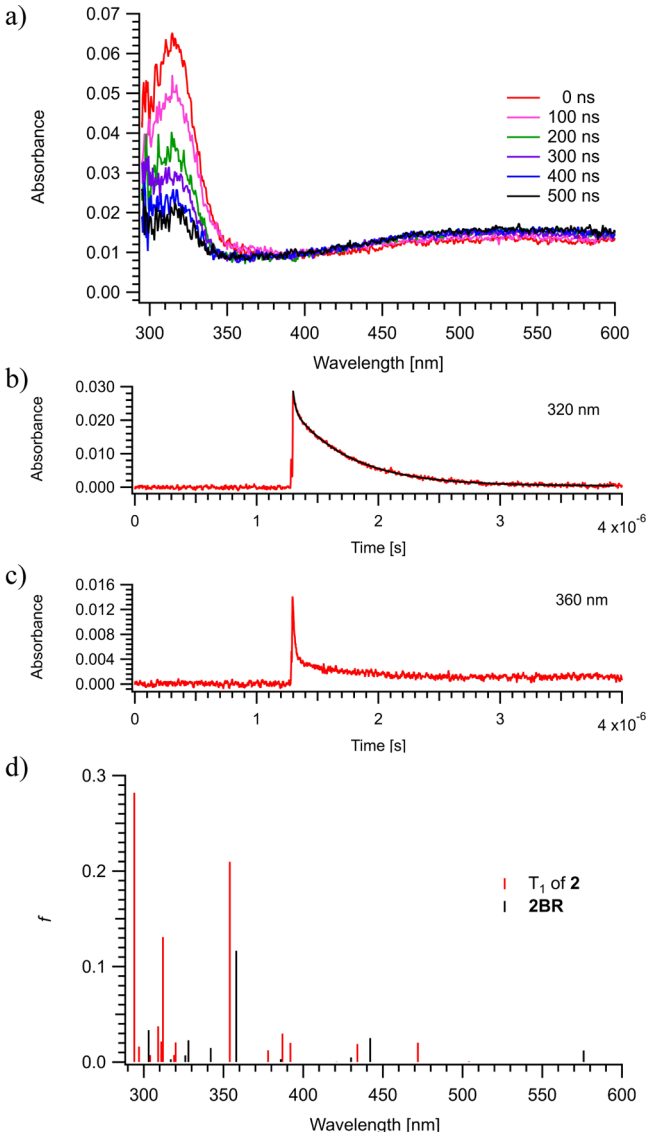

Figure 3. (a) Transient absorption spectra obtained by laser flash photolysis of **2** in argon-saturated acetonitrile using a 266 nm Nd:YAG laser. Kinetic traces at (b) 320 nm and (c) 360 nm obtained by laser flash photolysis of **2** in argon-saturated acetonitrile. (d) TD-DFT-calculated electronic transitions for $T_1$of **2**and **2BR**.

$\times$ 10^9 M^{-1} s^{-1} (Figure 4), thus revealing that T_1 of **2** is quenched with a rate constant similar to T_1 of **1**.

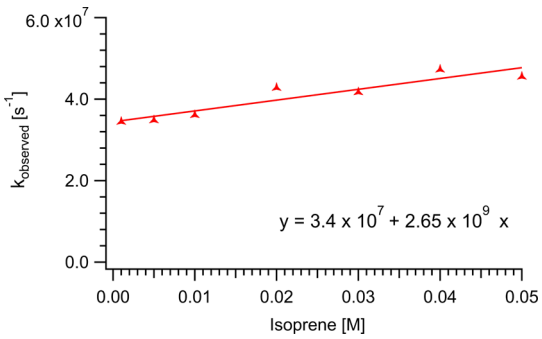

Figure 4. Quenching plot for the rate of decay of T_1 of **2** versus isoprene concentration (266 nm laser).

To further confirm that the long-lived transient is due to **2BR** and that it is formed from a triplet precursor T_1 of **2**, we studied the effect of isoprene on the intensity of the absorption at 360 nm. We performed the laser flash photolysis with a 308 nm excimer laser that has a time resolution of ~17 ns; therefore, we did not observe the absorption due to T_1 of **2** but only that due to **2BR** (λ_{max} ~ 360 nm, Figure 5). The higher

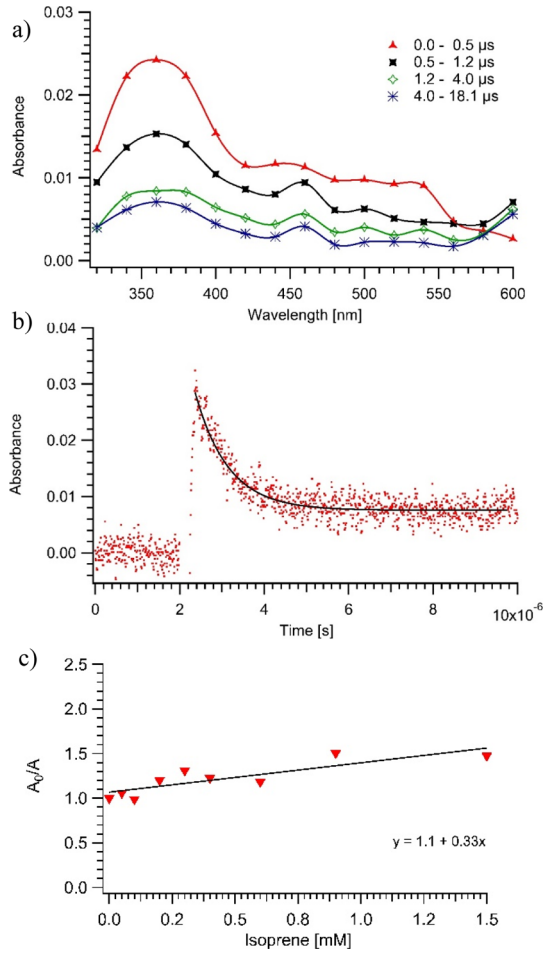

Figure 5. (a) Transient absorption spectra and (b) kinetic trace at 360 nm obtained by laser flash photolysis of ketone **2** in argon-saturated acetonitrile using a 308 nm excimer laser. (c) Stern–Volmer plot for quenching the absorption of **2BR** at 360 nm with isoprene.

concentration needed for the 308 nm irradiation prevented detection of transient absorption below 320 nm. The intensity of the absorption of **2BR** and the rate of decay at 360 nm were measured as a function of isoprene concentration. The intensity of the absorption decreased as the concentration of isoprene increased without significantly affecting the rate of decay. A Stern–Volmer plot of the absorption (A_0) without any isoprene divided by the absorption (A) at each isoprene concentration versus the concentration of isoprene shows a straight line with intercept of 1.1 (Figure 5c). We used the Stern–Volmer equation (eq 1) to estimate the lifetime τ (τ_0) of the precursor to triplet **2BR**, that is, T_1 of **2**.

$$\frac{A_0}{A} = 1 + k_q\tau_0[Q] \tag{1}$$

Using the slope of the straight line, the lifetime (τ_0) of T_1 of **2** was obtained as being between 3.3 and 33 ns by assuming

https://dx.doi.org/10.1021/acs.jpca.0c04319
J. Phys. Chem. A 2020, 124, 7346−7354

that the quenching was diffusion-controlled, that is, k_q is between 10^9 and 10^{10} M^{-1} s^{-1}. This result fits well with the directly observed lifetime of T_1 of **2** (~ 20 ns). Thus, the quenching studies further support that **2BR** is formed from T_1 of **2**.

3.3. Phosphorescence. The phosphorescence of ketones **1** and **2** was obtained in frozen ethanol matrices at 77 K. The phosphorescence spectrum for ketone **1** exhibited a vibrational structure (Figure 6), similar to that typically observed for

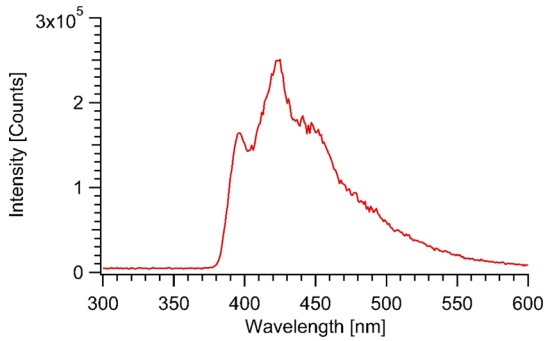

Figure 6. Phosphorescence spectrum of ketone **1** in ethanol at 77 K.

triplet ketones with (n, π^*) configurations. The first vibrational band was located at 396 nm for ketone **1**, which corresponds to a (0,0) band of 72 kcal/mol. The emission spectrum of ketone **2** did not exhibit well-resolved emission bands, but the emission onset occurred at 395 nm, which also corresponds to a (0,0) band of 72 kcal/mol. These energies correspond to the triplet excited state energy of *p*-methoxyacetophenone.[31]

3.4. Calculations. To support the proposed mechanism in Scheme 3, we calculated stationary points on the triplet surfaces of ketones **1** and **2** using the B3LYP level of theory and the 6-31+G(d) basis set.[12,32]

The optimized structure (B3LYP/6-31G+(d)) of the ground state (S_0) of ketone **1** showed that the acetophenone moiety, the vinyl bond, and the ester group are conjugated (Figure 7a).

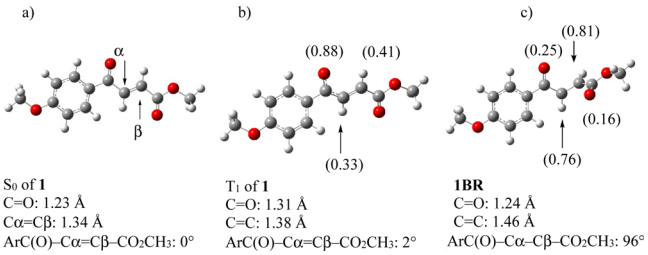

Figure 7. Bond lengths, spin densities (in parenthesis), and torsion angles of (a) **1**, (b) T_1 of **1**, and (c) **1BR**.

Single-point TD-DFT calculations on the optimized structure of S_0 of **1** place the vertical energies of S_1 and T_1 of **1** at 72 and 61 kcal/mol, respectively, above its S_0. In comparison, the energy of the optimized structure of T_1 of **1** is somewhat lower (55 kcal/mol above the S_0 of **1**). As shown in Figure 7, the C═O bond in the optimized structure of T_1 of **1** (1.31 Å) is elongated in comparison to that in S_0 of **1** (1.23 Å), as is generally observed for the triplet excited states of ketones with a (n, π^*) configuration.[33,34] In addition, the spin density calculations demonstrated that the unpaired electrons are mainly located on the carbonyl O atom (0.88) and the vinylic Cα (0.33) and Cβ (0.41) atoms (Figure 7b), thus verifying that T_1 of **1** is best described as a triplet vinyl ketone with a (n, π^*) configuration.

It should be noted that B3LYP calculations have been reported to underestimate the energies of optimized structures of triplet ketones with (n, π^*) configurations, whereas TD-DFT calculations estimate these energies more accurately.[35] However, the energy obtained from the phosphorescence spectrum of ketone **1** is considerably higher than the energies obtained either from the optimized structure or from TD-DFT calculations for T_1 of **1**. Thus, we speculate that the emission is not from T_1 of **1**, but is rather due to a higher excited state of ketone **1** that resembles T_1 of *p*-methoxyacetophenone.[30]

The optimized structure of **1BR** had a Cα−Cβ bond length of 1.46 Å and an ArC(O)−Cα−Cβ−CO_2CH_3 torsion angle of 96° (Figure 7c). Furthermore, because the spin density calculations demonstrated that the unpaired electrons are located mainly on the Cα and Cβ atoms (Figure 7c), it can be concluded that **1BR** is best described as a twisted triplet 1,2-biradical with the two radical centers orthogonal to each other.

In addition, we calculated the rotational barrier for T_1 of **1** around the vinylic bond (ArC(O)−Cα═Cβ−CO_2CH_3) (Figure 8). It was found that T_1 of **1** can rotate into **1BR**, and there is only a small rotational barrier of 2.3 kcal/mol for T_1 of **1** to form **1BR**.

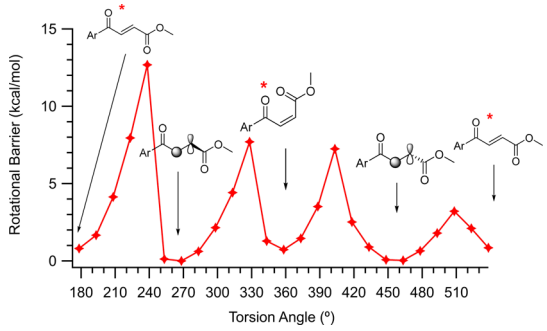

Figure 8. Calculated rotational barrier around the ArC(O)−Cα═Cβ−CO_2CH_3 bond in T_1 of **1**.

The structure of ketone **2** was also optimized, which revealed that the ester moiety is conjugated with the vinyl bond, as the O═C(O_2CH_3)−Cα═Cβ torsion angle is −1°, whereas the ketone is orthogonal to the vinyl bond, as the O═C(Ar)−Cα═Cβ torsion angle is −100° (Figure 9a). The optimized structure of **2** is similar to the X-ray structure of ketone **2** with the key torsion angles O2−C2−C3−C8 = −9.7(2)°, C9−C8−C3−C2 = 9.5(2)°, C10−C9−C8−C3 = −90.6(1)°, and O3−C9−C8−C3 = 96.1(1)° (Figure 9b). Presumably, the steric interaction between the two vinyl

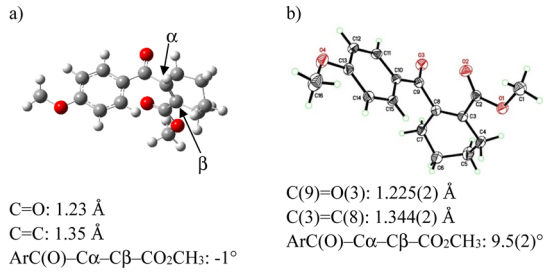

Figure 9. (a) Optimized structure and (b) X-ray structure of ketone **2**.

https://dx.doi.org/10.1021/acs.jpca.0c04319
J. Phys. Chem. A 2020, 124, 7346−7354

substituents forces the ketone to be out of conjugation with the vinylic bond.

Single-point TD-DFT (B3LYP/6-31+G(d)) on the optimized structure of S_0 of **2** placed the vertical energies of S_1 and T_1 of **2** at 88 and 72 kcal/mol, respectively, above its S_0. In comparison, the optimized structure of T_1 of **2** is located 59 kcal/mol above its S_0. Because the (B3LYP/6-31+G(d)) optimized structure of T_1 of **2** has an elongated C═O bond of 1.30 Å and the spin density calculations place the unpaired electron density mainly on the carbonyl O atom, T_1 of **2** is best described as a triplet ketone with a (n, π^*) configuration (Figure 10a). The calculated ArC(O)−Cα−Cβ−CO_2CH_3

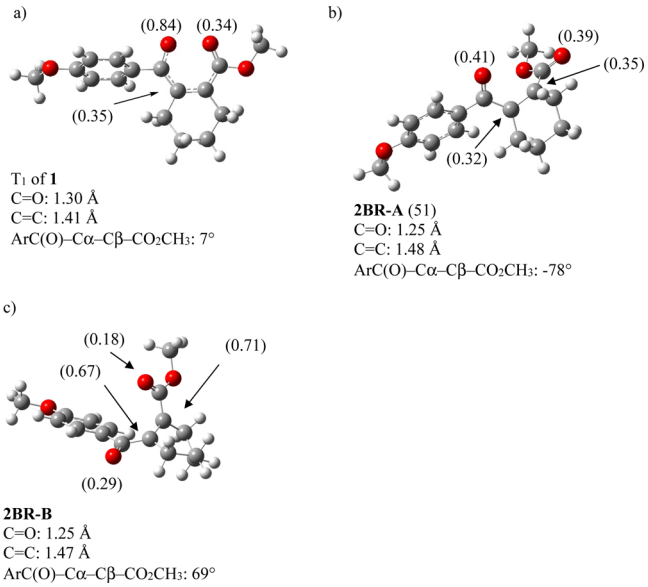

Figure 10. Bond lengths, spin densities (in parenthesis), and torsion angles of (a) T_1 of **1**, (b) triplet **2BR-A**, and (c) triplet **2BR-B**.

torsion angle is 7° as the ester group is conjugated with the C═O group, but the p-methoxyphenyl group is rotated −60° out of conjugation with the C═O group, which permits the ester group to be conjugated with the vinyl bond and the ketone. In addition, the optimized structures of T_1 of **2** and **2** are different, whereas the structures of T_1 of **1** and **1** are similar, and thus, the energies for T_1 of **2** obtained from optimization and single point TD-DFT calculations are more different, than for T_1 of **1**.

We optimized two minimal energy conformers of **2BR** (**2BR-A** and **2BR-B**, with **2BR-B** being 3 kcal/mol higher in energy, Figure 10b,c). The optimized structure of **2BR-A** has a torsional angle (ArC(O)−Cα−Cβ−CO_2CH_3) of −78°, which results in the two carbon-centered radicals being twisted away from each other (Figure 10b). Spin density calculations revealed that the spin densities of vinylic Cα and Cβ atoms in **2BR-A** (0.32 and 0.35, respectively) are lower than those of the carbonyl O atom (0.41) and the ester carbonyl O atom (0.39). Thus, the biradical centers in **2BR-A** are stabilized by conjugation with the carbonyl and ester groups. In comparison, in the optimized structure of conformer **2BR-B**, the unpaired spin density is mainly located on the Cα and Cβ atoms (0.67 and 0.71, respectively), with a small amount on the two carbonyl O atoms (Figure 10c). Moreover, the ArC(O)−Cα−Cβ−CO_2CH_3 torsion angle of **2BR-B** is smaller (69°). Presumably, in conformer **2BR-A**, the biradical centers are closer to being orthogonal to each other and thus are more stabilized than those in **2BR-B**.

The rotational barrier for T_1 of **2** around its vinylic bond was calculated (Figure 11). Obviously, T_1 of **2** cannot rotate into

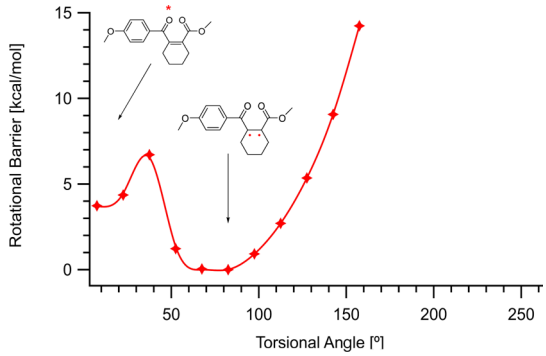

Figure 11. Calculated rotational barrier around the ArC(O)−Cα═Cβ−CO_2CH_3 bond in T_1 of **2**.

its cis-isomer because it is conformationally locked by the ring structure despite T_1 of **2** having a small rotational barrier of ∼3 kcal/mol to form **2BR**.

Finally, we compared stationary points on the energy diagrams of ketones **1** and **2**, as shown in Figure 12. The

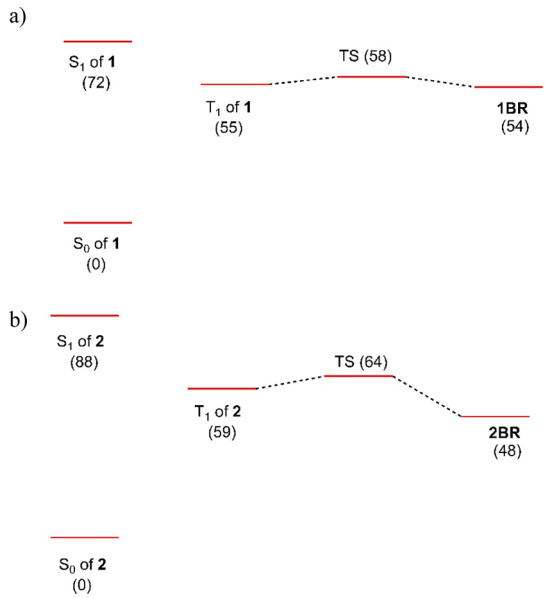

Figure 12. Calculated stationary points on the triplet surface of (a) ketone **1** and (b) ketone **2**. The energies of S_1 are obtained by single-point TD-DFT calculations, whereas the energies for S_0, T_1, TS and BR are obtained from their optimized structures using B3LYP/6-31G +(d). Energies are in kcal/mol.

transition-state barriers for T_1 of **1** and T_1 of **2** forming corresponding biradicals **1BR** and **2BR** are only a few kilocalories per mol. Thus, the transition states are expected to be easily accessible at ambient temperature.

4. DISCUSSION

The laser flash photolysis results demonstrate that T_1 of **1** and T_1 of **2** are short-lived because they decay efficiently to form biradicals **1BR** and **2BR**, respectively. The calculated transition state for T_1 of **1** to form **1BR** and the rotational barrier for T_1

https://dx.doi.org/10.1021/acs.jpca.0c04319
J. Phys. Chem. A 2020, 124, 7346−7354

Scheme 4. Comparison of calculated spin Densities for Twisted Triplet 1,2-Biradicals 1BR, 2BR, 3BR, and 4BR

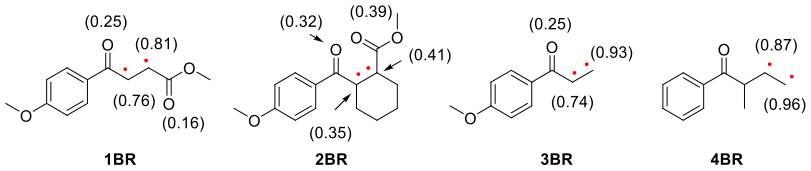

of **1** to rotate into **1BR** are similar, indicating that only ∼3 kcal/mol is required to transform T_1 of **1** to **1BR**. In comparison, the calculated transition-state barrier for T_1 of **2** to form **2BR** is larger (5 kcal/mol); however, the calculated rotational barrier for T_1 of **2** to rotate into **2BR** is just ∼3 kcal/mol.

We compared the photoreactivities of ketones **1** and **2** to those of ketones **3** and **4** (Scheme 4), which are also simple alkenes with a built-in triplet sensitizer, to better address the effect of conjugation of the vinylic bonds in ketones **1** and **2**. The vinylic bond in ketone **3** is conjugated only to an acetophenone moiety, and in ketone **4**, it does not have any conjugation. Irradiation of ketone **3**, with a deuterium label in the β-position, yields the corresponding cis-isomer through the formation of a twisted triplet biradical **3BR**. Laser flash photolysis results show that both **3BR** and **4BR** have lifetimes of a few microseconds.[10,11] A comparison of the calculated spin densities shows similarities for **1BR** and **3BR** (Scheme 4), with the majority of the spin density located on the Cα and Cβ carbon atoms and a small amount located at the ketone and the ester carbonyl O atoms. In contrast, in **4BR**, all the spin density is located on the Cα and Cβ carbon atoms because the vinylic bond is not conjugated. Furthermore, the calculated rotational barrier of the vinylic bond in **4BR** is ∼16 kcal/mol, which is significantly larger than the corresponding rotational barriers for **1BR** and **2BR**.[10,11] As the vinylic bond in ketone **1** is conjugated at both terminals, the calculated rotational barrier around the vinylic bond from T_1 of **1** to **1BR** is smaller because both the radical centers are stabilized by conjugation. Thus, we theorize that the flexibility of **1BR** allows it to rotate into a conformer that is favorable for intersystem crossing to its S_0.

In contrast to those of **1BR**, **3BR**, and **4BR**, the spin densities of the minimal energy structure of biradical **2BR** are significantly different, with similar spin densities on the Cα, Cβ, and carbonyl O atoms. Moreover, the ArC(O)−Cα−Cβ−CO_2CH_3 torsion angle in **2BR** is approximately −78°. Thus, biradical **2BR** adopts a configuration in which the two radical centers are fully conjugated with the carbonyl O atoms, presumably to relieve steric interactions between the substituents on the Cα and Cβ atoms, while keeping the radical centers on the Cα and Cβ atoms close to orthogonal. As a result, **2BR** is not as flexible as **1BR**, and therefore, it does not intersystem-cross as effectively to its S_0.

5. CONCLUSIONS

We have demonstrated that upon irradiation, ketones **1** and **2** form T_1 of **1** and T_1 of **2**, respectively. We conclude that T_1 of **1** is short-lived because it decays into biradical **1BR**, which efficiently intersystem-crosses to form *cis*- and *trans*-**1**. In this case, the rate-determining step is the decay of T_1 of **1** because the conjugation of the vinylic C atoms in biradical **1BR** reduces its rotational barrier to adopt a conformer for which intersystem crossing is efficient. In comparison, biradical **2BR** is more rigid owing to its cyclic structure and thus it cannot rotate easily into a conformer that allows efficient intersystem crossing to the ground state.

■ ASSOCIATED CONTENT

Supporting Information

The Supporting Information is available free of charge at https://pubs.acs.org/doi/10.1021/acs.jpca.0c04319.

NMR and IR spectra of **1** and **2**; Cartesian coordinates and energies of **1**, **2**, T_1 of **1**, T_1 of **2**, **1BR**, and **2BR** (PDF)

Crystallographic details for **2** (CIF)

■ AUTHOR INFORMATION

Corresponding Author

Anna D. Gudmundsdottir − *Department of Chemistry, University of Cincinnati, Cincinnati, Ohio 45221-0172, United States;* orcid.org/0000-0002-5420-4098; Phone: 513-556-3380; Email: anna.gudmundsdottir@uc.edu

Authors

Sujan K. Sarkar − *Department of Chemistry, University of Cincinnati, Cincinnati, Ohio 45221-0172, United States;* orcid.org/0000-0002-8471-6297

Ranaweera A. A. Upul Ranaweera − *Department of Chemistry, University of Cincinnati, Cincinnati, Ohio 45221-0172, United States;* orcid.org/0000-0003-1614-1919

Rajkumar Merugu − *Department of Chemistry, University of Cincinnati, Cincinnati, Ohio 45221-0172, United States*

Nayera M. Abdelaziz − *Department of Chemistry, University of Cincinnati, Cincinnati, Ohio 45221-0172, United States*

Jendai Robinson − *Department of Chemistry, University of Cincinnati, Cincinnati, Ohio 45221-0172, United States*

Heidi A. Day − *Department of Chemistry, University of Cincinnati, Cincinnati, Ohio 45221-0172, United States*

Jeanette A. Krause − *Department of Chemistry, University of Cincinnati, Cincinnati, Ohio 45221-0172, United States*

Complete contact information is available at: https://pubs.acs.org/10.1021/acs.jpca.0c04319

Author Contributions

†S.K.S. R.A.A.U.R. and R. M. contributed equally.

Notes

The authors declare no competing financial interest.

■ ACKNOWLEDGMENTS

The authors thank the National Science Foundation (CHE-1800140 & MRI-CHE-1726092) and the OSC (PES0597). J.R. is grateful for an NSF-REU fellowship (CHE-0452387). S.K.S. acknowledge Doctoral Enhancement Fellowship, R.A.A.U.R. URC and Ann P. Villalobos Fellowships and N.M.A. Halshall Fellowship from the Chemistry Department at UC. Crystallographic data were collected through the SCrALS (Service Crystallography at Advanced Light Source) program

at Beamline 11.3.1 at the Advanced Light Source (ALS), Lawrence Berkeley National Laboratory. The ALS is supported by the U.S. Department of Energy, Office of Energy Sciences Materials Sciences Division, under contract DE-AC02-05CH11231.

■ REFERENCES

(1) Dugave, C.; Demange, L. Cis−Trans Isomerization of Organic Molecules and Biomolecules: Implications and Applications. *Chem. Rev.* **2003**, *103*, 2475−2532.

(2) García-López, V.; Liu, D.; Tour, J. M. Light-Activated Organic Molecular Motors and Their Applications. *Chem. Rev.* **2020**, *120*, 79−124.

(3) Sankaranarayanan, J.; Muthukrishnan, S.; Gudmundsdottir, A. D. Photoremovable Protecting Groups Based on Photoenolization. In *Advances in Physical Organic Chemistry*; Richard, J. P., Ed.; Academic Press: Amsterdam, 2009; Vol. *43*, pp 39−77.

(4) Klán, P.; Šolomek, T.; Bochet, C. G.; Blanc, A.; Givens, R.; Rubina, M.; Popik, V.; Kostikov, A.; Wirz, J. Photoremovable Protecting Groups in Chemistry and Biology: Reaction Mechanisms and Efficacy. *Chem. Rev.* **2013**, *113*, 119−191.

(5) Merino, E.; Ribagorda, M. Control over Molecular Motion Using the Cis−Trans Photoisomerization of the Azo Group. *Beilstein J. Org. Chem.* **2012**, *8*, 1071−1090.

(6) Caldwell, R. A. Intersystem Crossing in Organic Photochemical Intermediates. *Pure Appl. Chem.* **1984**, *56*, 1167−1177.

(7) Unett, D. J.; Caldwell, R. A. The Triplet State of Alkenes: Structure, Dynamics, Energetics and Chemistry. *Res. Chem. Intermed.* **1995**, *21*, 665−709.

(8) Caldwell, R. A.; Cao, C. V. Structural Effects on Twisted Olefin Triplet Lifetimes. Styrene Derivatives. *J. Am. Chem. Soc.* **1982**, *104*, 6174−6180.

(9) García-Expósito, E.; González-Moreno, R.; Martín-Vilà, M.; Muray, E.; Rifé, J.; Bourdelande, J. L.; Branchadell, V.; Ortuño, R. M. On the Z−E Photoisomerization of Chiral 2-Pentenoate Esters: Stationary Irradiations, Laser-Flash Photolysis Studies, and Theoretical Calculations. *J. Org. Chem.* **2000**, *65*, 6958−6965.

(10) Sriyarathne, H. D. M.; Thenna-Hewa, K. R. S.; Scott, T.; Gudmundsdottir, A. D. Formation and Direct Detection of Non-Conjugated Triplet 1,2-Biradical from β,γ-Vinylarylketone. *Aust. J. Chem.* **2015**, *68*, 1707−1714.

(11) Ranaweera, R. A. A. U.; Scott, T.; Li, Q.; Rajam, S.; Duncan, A.; Li, R.; Evans, A.; Bohne, C.; Toscano, J. P.; Ault, B. S.; et al. Trans−Cis Isomerization of Vinylketones through Triplet 1,2-Biradicals. *J. Phys. Chem. A* **2014**, *118*, 10433−10447.

(12) Lee, C.; Yang, W.; Parr, R. G. Development of the Colle-Salvetti Correlation-Energy Formula into a Functional of the Electron Density. *Phys. Rev. B: Condens. Matter Mater. Phys.* **1988**, *37*, 785−789.

(13) Frisch, M. J.; Trucks, G. W.; Schlegel, H. B.; Scuseria, G. E.; Robb, M. A.; Cheeseman, J. R.; Scalmani, G.; Barone, V.; Petersson, G. A.; Nakatsuji, et al. *Gaussian 16* Rev. C.01; Gaussian Inc.: Wallingford, CT, 2016.

(14) Bauernschmitt, R.; Ahlrichs, R. Treatment of Electronic Excitations within the Adiabatic Approximation of Time Dependent Density Functional Theory. *Chem. Phys. Lett.* **1996**, *256*, 454−464.

(15) Stratmann, R. E.; Scuseria, G. E.; Frisch, M. J. An Efficient Implementation of Time-Dependent Density-Functional Theory for the Calculation of Excitation Energies of Large Moleculesr. *J. Chem. Phys.* **1998**, *109*, 8218−8224.

(16) Foresman, J. B.; Head-Gordon, M.; Pople, J. A.; Frisch, M. J. Toward a Systematic Molecular Orbital Theory for Excited States. *J. Phys. Chem.* **1992**, *96*, 135−149.

(17) Klamt, A.; Schüürmann, G. COSMO: A New Approach to Dielectric Screening in Solvents with Explicit Expressions for the Screening Energy and Its Gradient. *J. Chem. Soc., Perkin Trans. 2* **1993**, 799−805.

(18) Barone, V.; Cossi, M. Quantum Calculation of Molecular Energies and Energy Gradients in Solution by a Conductor Solvent Model. *J. Phys. Chem. A* **1998**, *102*, 1995−2001.

(19) Cossi, M.; Rega, N.; Scalmani, G.; Barone, V. Energies, Structures, and Electronic Properties of Molecules in Solution with the C-PCM Solvation Model. *J. Comput. Chem.* **2003**, *24*, 669−681.

(20) Gonzalez, C.; Schlegel, H. B. An Improved Algorithm for Reaction Path Following. *J. Chem. Phys.* **1989**, *90*, 2154−2161.

(21) Gonzalez, C.; Schlegel, H. B. Reaction Path Following in Mass-Weighted Internal Coordinates. *J. Phys. Chem.* **1990**, *94*, 5523−5527.

(22) Muthukrishnan, S.; Sankaranarayanan, J.; Klima, R. F.; Pace, T. C. S.; Bohne, C.; Gudmundsdottir, A. D. Intramolecular H-Atom Abstraction in γ-Azido-Butyrophenones: Formation of 1,5 Ketyl Iminyl Radicals. *Org. Lett.* **2009**, *11*, 2345−2348.

(23) Drakulić, B. J.; Stanojković, T. P.; Žižak, Ž. S.; Dabović, M. M. Antiproliferative Activity of Aroylacrylic Acids. Structure-Activity Study Based on Molecular Interaction Fields. *Eur. J. Med. Chem.* **2011**, *46*, 3265−3273.

(24) Tolstoluzhsky, N.; Nikolaienko, P.; Gorobets, N.; Van der Eycken, E. V.; Kolos, N. Efficient Synthesis of Uracil-Derived Hexa- and Tetrahydropyrido[2,3-d]pyrimidines. *Eur. J. Org. Chem.* **2013**, *2013*, 5364−5369.

(25) Xu, C.; Bai, X.; Xu, J.; Ren, J.; Xing, Y.; Li, Z.; Wang, J.; Shi, J.; Yu, L.; Wang, Y. Substituted 4-Oxo-Crotonic Acid Derivatives as a New Class of Protein Kinase B (PknB) Inhibitors: Synthesis and Sar Study. *RSC Adv.* **2017**, *7*, 4763−4775.

(26) Barr, K. P.; Dean, F. M.; Locksley, H. D. Condensation Products of Maleic Anhydride with Phenols. *J. Chem. Soc.* **1959**, 2425−2430.

(27) Papa, D.; Schwenk, E.; Villani, F.; Klingsberg, E. α-Bromination of Dicarboxylic Acids. *J. Am. Chem. Soc.* **1948**, *70*, 3626−3627.

(28) Sonye, J. P.; Koide, K. Sodium Bicarbonate-Catalyzed Stereoselective Isomerizations of Electron-Deficient Propargylic Alcohols to (Z)-Enones. *J. Org. Chem.* **2007**, *72*, 1846−1848.

(29) Small, R. D., Jr.; Scaiano, J. C. Differentiation of Excited-State and Biradical Processes. Photochemistry of Phenyl Alkyl Ketones in the Presence of Oxygen. *J. Am. Chem. Soc.* **1978**, *100*, 4512−4519.

(30) Boch, R.; Bohne, C.; Scaiano, J. C. Time-Resolved Diffuse Reflectance Studies of β-Phenyl Ketones in the Solid State: Conformational and Chiral Control of Triplet Lifetimes. *J. Org. Chem.* **1996**, *61*, 1423−1428.

(31) Yang, N.-C.; McClure, D. S.; Murov, S.; Houser, J. J.; Dusenbery, R. Photoreduction of Acetophenone and Substituted Acetophenones. *J. Am. Chem. Soc.* **1967**, *89*, 5466−5468.

(32) Becke, A. D. Density-Functional Thermochemistry. III. The Role of Exact Exchange. *J. Chem. Phys.* **1993**, *98*, 5648−5652.

(33) Srivastava, S.; Yourd, E.; Toscano, J. P. Structural Differences between $\pi\pi^*$ and nπ^* Acetophenone Triplet Excited States as Revealed by Time-Resolved Ir Spectroscopy. *J. Am. Chem. Soc.* **1998**, *120*, 6173−6174.

(34) Fang, W.-H.; Phillips, D. L. The Crucial Role of the $S_1/T_2/T_1$ Intersection in the Relaxation Dynamics of Aromatic Carbonyl Compounds Upon n→π^* Excitatio. *ChemPhysChem* **2002**, *3*, 889−892.

(35) Muthukrishnan, S.; Mandel, S. M.; Hackett, J. C.; Singh, P. N. D.; Hadad, C. M.; Krause, J. A.; Gudmundsdóttir, A. D. Competition between α−Cleavage and Energy Transfer in α−Azidoacetophenones. *J. Org. Chem.* **2007**, *72*, 2757−2768.

https://dx.doi.org/10.1021/acs.jpca.0c04319
J. Phys. Chem. A 2020, 124, 7346−7354